

A Theoretical Investigation of the Detection of Vital Signs in Presence of Car Vibrations and RADAR-Based Passenger Classification

Steve Dias Da Cruz^{ID}, Hans-Peter Beise, Udo Schröder, and Una Karahasanovic

Abstract—The observation of the passenger compartment using an interior RADAR becomes challenging when a vehicle is in motion. The signal received by the RADAR sensor measures not only the target’s motion that we would like to detect, e.g., vital signs, but also a second, unwanted motion induced by exterior effects, e.g., displacement caused by the road, strong wind gusts, or car engine vibrations. Consequently, traditional techniques used to remove white Gaussian noise cannot be applied in this scenario. We propose a theoretical framework to investigate the denoising of a signal received by an interior RADAR using accelerometer measurements and a mechanical model to generate the cancellation signal stemming from the (unwanted) vibrational motion. We explain the denoising technique and show that the fundamental idea behind the cleaning process works well. Our observations are corroborated by a robust mathematical model and verified by simulations. Furthermore, the aforementioned denoising techniques enable us to formulate and solve an optimization problem to find an estimation for the passenger’s mass in certain cases.

Index Terms—Accelerometers, automotive applications, Doppler measurement, optimization, RADAR, signal denoising, vehicle driving, vehicle dynamics.

I. INTRODUCTION

THE use of RF-signals for vital sign monitoring [1] has been a topic of intense research. This is due to the promising and versatile applications of these systems, for example in medical applications [2], for the detection of buried people in disaster-affected areas [3], for through-the-wall detection [4] or in automotive industry [5], [6]. In this work, we focus on the automotive application. The relevance and implementation of such a system for the detection of children forgotten in a car is elaborated [5]. Due to the ever growing interest in autonomous driving, the topic of vital sign monitoring in a moving car has become very important [6]. Not only can an interior car RADAR detect passengers and their motions, but it is also capable of

Manuscript received May 15, 2018; revised October 22, 2018; accepted January 15, 2019. Date of publication February 11, 2019; date of current version April 16, 2019. This work was supported in part by the University of Luxembourg, in part by the MECO “Advanced millimeter-wave technologies for imaging applications” project under Grant Ind. 446.04.RED.14.49 CVN 33/14/RED CW, and in part by IEE S.A. The review of this paper was coordinated by Dr. S. Anwar. (Corresponding author: Steve Dias Da Cruz.)

The authors are with the IEE S.A., ZAE Weiergewan 11, Contern L-5326, Luxembourg (e-mail: steve.dias-da-cruz@iee.lu; hans-peter.beise@iee.lu; una.karahasanovic@iee.lu; udo.schroeder@iee.lu).

Digital Object Identifier 10.1109/TVT.2019.2898512

monitoring respiratory motion and heart-rate [1]. However, the received signal will not only contain information about the passenger’s vital signs, but it will also contain information about the passenger’s motion induced by the movement of a driving car. Consequently, it becomes rather challenging to monitor vital-signs in a non-stationary environment using a RADAR-based sensor.

In order to overcome this problem, we propose to attach an accelerometer to the RADAR-based sensor [7] to gain information about the unwanted motion of the car-body caused by exterior influences. Knowledge about the motion of the RADAR sensor enables us to extract useful information for the denoising process. Using these measurements enables us to reconstruct the dynamics of the seat and the passenger, provided that the mechanical model and its parameters are known. This dynamics can then be used to calculate the contribution to the Doppler frequency of the received wave, which can then be subtracted off the received signal. In this way, one is left with an (almost) clean signal, containing only information about vital signs.

However, in order to correctly describe the influence of these exterior effects on the dynamics of the seat and the passenger, we need to develop a good approximation of the passenger’s weight as it is one of the relevant parameters in corresponding mechanical models. We formulate an optimization problem, which is solved using the previously mentioned denoising technique, to find a good estimation of the passenger’ mass. The corresponding objective function is designed to achieve an extremum when the denoised RADAR signal shows signatures of breathing [8]. Once a good estimation is found, the corresponding mass can then be used to denoise the received signal. Additionally, the estimated weight can also be used as input for other systems, for instance, to adapt the intensity of air bag deployment and thereby to reduce possible injuries [9].

In Section II we define the simulation environment and establish a mechanical model to describe the transmission of a random road profile into seat vibrations in the passenger compartment in order to obtain the resulting disturbance on the breathing motion of a passenger. In Section III we introduce and prove the denoising method using accelerometer measurements of the unwanted vibrational motion. In Section IV we investigate the mathematical foundation of the proposed physical model of Section II and we perform a sensitivity analysis of the latter in order to understand the origin, boundedness and controllability of possible errors. Finally, in Section V we propose to combine

information about the system's vibrations with the proposed denoising method of Section III to formulate and solve an optimization problem in order to determine the passenger's weight using interior RADAR. The main result is the introduction of a mathematical framework to analyze possible robust denoising methods to remove the contribution of unwanted exterior motion from the received RADAR signal using accelerometer measurements. One can also use the latter method to find an estimation of the passenger's mass with a relative error of less than ten percent once one manages to get a good understanding of the physics of the vehicle's interior.

A. Signal Received by the Interior RADAR-Based Sensor

For a continuous-wave (CW) RADAR system detecting the echo of a point target P , the instantaneous signal $u_r(t)$ received, after having passed the low-pass filter and the mixer, is given by [10]

$$u_r(t) = \rho(t) e^{-i \frac{4\pi}{\lambda} r(t)}, \quad (1)$$

where $\rho(t)$ is the instantaneous amplitude (which will not be examined in detail in what follows, as we are only interested in the Doppler frequency), λ is the carrier wavelength and $r(t)$ is the instantaneous distance between the RADAR and the target. Consequently, when the point target is undergoing multiple motions simultaneously, where one of the motions is unwanted, then this unwanted motion affects the term $r(t)$ of the received signal. Hence, the disturbance of the signal cannot be simply modelled as superimposed noise or clutter, as it is commonly considered, for instance, in wavelet denoising methods [11].

II. MODEL SETUP

We will introduce a simple, but sufficiently realistic simulation environment that enables us to simulate the noise and test the validity of the aforementioned denoising method. Since we need to simulate the noise emerging from motion of the observed target due to external (e.g., road) influences, we introduce a model to generate a realistic road profile, which causes the car body to undergo (various) vibrational motions. We formulate a mechanical model, which takes the road profile as an input and outputs the seat displacement of the passenger compartment. The target then undergoes two motions: the displacement caused by the seat movement and the respiratory motion, which we would like to detect. In order to simulate electromagnetic waves and their propagation and reflection, we use a MATLAB-based simulation environment developed with the aid of the Phased Array System Toolbox [12].

In addition, all our simulations take into account the presence of random thermal noise. However, we found that the thermal noise does not affect the proposed denoising method due to the high processing gain of the Fast Fourier Transform (FFT) ($10 \log_{10}(\frac{\sigma}{2})$ dB, where σ is the length of the FFT [13]). Additionally, the comparatively small distance (typically smaller than 1m) between the RADAR device and the target results in a rather high signal strength and therefore also a higher signal to noise ratio.

TABLE I
ROAD ROUGHNESS ISO CATEGORIZATION

Road Class	$\Phi(\Omega_0)(10^{-6} m^3)$, $\Omega_0 = 1$
A (very good)	1
B (good)	4
C (average)	16
D (poor)	64
E (very poor)	256

A. Road Profile

As proposed and investigated in [14], we use a Fourier type approximation to simulate a one-dimensional random road profile. The latter is used by the quarter car model, which takes the street roughness as an input, and calculates (outputs) the resulting mechanical movement of the seat. The road profiles are classified using the ISO 8606 standard, and they are modelled as a superposition of N ($\rightarrow \infty$) sine waves

$$z_R(s) = \sum_{i=1}^N A_i \sin(\Omega_i s - \phi_i), \quad (2)$$

where s is the location on the road and where the amplitudes A_i are defined by

$$A_i = \sqrt{\Phi(\Omega_i) \frac{\Delta\Omega}{\pi}} \quad i = 1, \dots, N, \quad (3)$$

in which $\Delta\Omega = \frac{\Omega_N - \Omega_1}{N-1}$ (rad/s). We chose $\Omega_0 = 1$ (rad/m), $\Omega_1 = 0.02\pi$ (rad/m) and $\Omega_N = 6\pi$ (rad/m), Ω_i for $i = 1, \dots, N$ form an equidistant subdivision of $[\Omega_1, \Omega_N]$. The phase angles ϕ_i for $i = 1, \dots, N$ are random variables following a uniform distribution in the interval $[0, \pi]$ and

$$\Phi(\Omega) = \Phi(\Omega_0) \left(\frac{\Omega}{\Omega_0} \right)^{-2}, \quad \text{for } \Omega_1 < \Omega \leq \Omega_N, \quad (4)$$

which describes the road roughness and the fact that large amplitude road bumps occur with smaller frequency and vice versa. The value for $\Phi(\Omega_0)$ depends on the roughness of the street that one wants to simulate. The ISO values are given in Table I. An example of a road profile of roughness class C using 1000 frequencies is shown in Fig. 1.

B. Mechanical Model

In order to obtain the displacement of the seat as a function of the road roughness, we are going to use a quarter car model, a simplified version of the half car model used in [15] and [16], given by a three-spring model. Since we are investigating the feasibility of the method itself, we will consider, for simplicity, only the displacement of the seat along the z-direction. The three-spring model is a coupled damped oscillator model with an excitation given by the road profile (2). Let us denote this excitation by y . In the following, and as depicted in Fig. 2, m_U , m_C and m_W denote, respectively, the mass of the seat/body (U), the car-body (C) and the wheel component (W). S_U , S_C and S_W are the corresponding stiffness constants, D_U , D_C and D_W

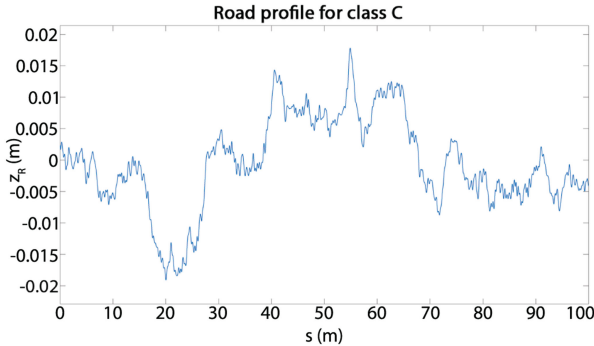


Fig. 1. Road profile of road roughness class *C*, given by (2), composed out of 1000 frequencies. z_R represents the (bump) amplitude, while s is the location on the (one-dimensional) road.

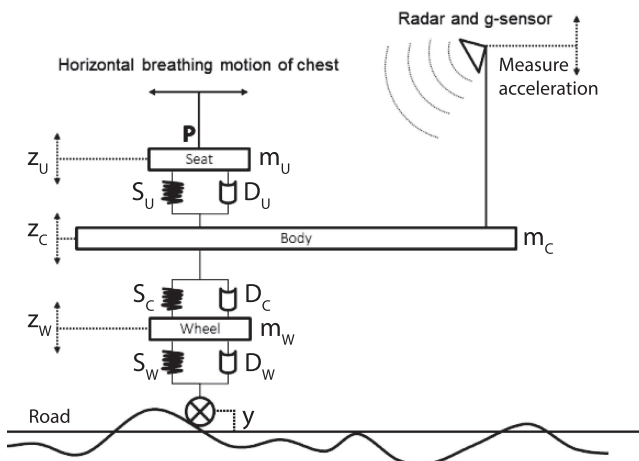


Fig. 2. The displacement along the z -direction of the wheel z_W , car-body z_C and seat z_U under the influence of a road profile y , given by (2), can be modeled by the three-spring model. The human chest is modeled as a point target P and is assumed to be rigidly attached to the seat. The chest undergoes a respiratory motion along x -direction and the displacement along the z -direction due to the road profile, which is assumed to be identical to the seat displacement. The RADAR sensor is assumed to be rigidly attached to the car body, which undergoes a different motion, z_C , due to the road profile. As a result, there is a small amount $z_C - z_U$ of relative motion between the RADAR sensor (moving with z_C) and the human chest (moving with z_U).

the damping constants and z_U , z_C and z_W the z -displacements of the seat/body (U), the car-body (C) and the wheel component (W). The resulting system of differential equations describing this motion is then

$$\begin{aligned} m_U \ddot{z}_U &= -D_U(\dot{z}_U - \dot{z}_C) - S_U(z_U - z_C), \\ m_C \ddot{z}_C &= S_C(z_W - z_C) + D_C(\dot{z}_W - \dot{z}_C) \\ &\quad + D_U(\dot{z}_U - \dot{z}_C) + S_U(z_U - z_C), \\ m_W \ddot{z}_W &= D_W \dot{y} + S_W y - (S_C + S_W)z_W \\ &\quad + S_C z_C - D_C(\dot{z}_W - \dot{z}_C). \end{aligned} \quad (5)$$

C. Respiratory Motion

The respiratory motion of the observed passenger is simulated by a cosine wave

$$x(t) = \alpha \cos(2\pi ft), \quad (6)$$

where $\alpha \in [0, 0.001, 0.012]$ m is the breathing amplitude and $f \in [0.2, 1.0]$ Hz is the breathing frequency. For comparison, a measurement of a recorded breathing motion can be found in [8]. The choice of the RADAR cross section (RCS) is not critical (in a meaningful interval) for our application, as the distance between the RADAR device and the target is relatively small (typically smaller than 1m). The RCS does not vary significantly enough (ranging from babies to adults) to have a critical impact on the RADAR measurements. The latter assumptions are supported by the application of RADAR based systems in the vehicle interior for the detection of sleeping babies [5]. In Fig. 3 we compare the simulations of received RADAR signals and spectrograms of two identical motions (same breathing pattern, same mass and identical road displacement) for two distinct RCS values: 0.34 m^2 (adult) [17] and 0.04 m^2 (baby) [18], in order to validate our assumptions. Although the ADC signal is noisier for the smaller RCS scenario, due to the high processing gain of the FFT, the resulting spectrograms are almost identical, because the noise is equally distributed among all frequencies for both RCS values. Consequently, since the algorithms we will propose in this work depend on the FFT and the resulting spectrograms, a smaller RCS will not affect our methods significantly. Another example, investigating the worst case scenario of a small baby (small RCS, small breathing amplitude and mass), is considered in Section V-D.

D. Point Target and RADAR Settings

In our simulations, we use, without loss of generality, a RADAR cross section (RCS) of 0.34 m^2 as a typical value for a human chest [17], [19], which we model as a point target P . The interior RADAR is then observing a point target P undergoing the periodic breathing motion along the x -direction and the displacement caused by the seat along the z -direction. This is depicted in Fig. 2. Consequently, the instantaneous position of the point target P is given by

$$P(t) = (x(t), 0, z_U(t)). \quad (7)$$

In our simulations, a continuous electromagnetic wave with a carrier frequency of $f_t = 79 \text{ GHz}$ is emitted. The sampling frequency was set to $f_s = 20 \text{ kHz}$.

E. Accelerometer

We assume that the wheel, the car-body and the seat are all undergoing different motions. The road profile is transformed into displacements of the aforementioned car parts by the spring damper system. Consequently, the seat experiences damped vibrations (they are smoother than the road profile, but have higher amplitudes). Furthermore, the seat motion will be affected by the passenger's mass. Hence, in order to get information about the vehicle interior motion, we record the acceleration \ddot{z}_C of the car-body during the simulation. It is assumed that the RADAR device is fixed to the car-body. In addition, we added random Gaussian noise and/or systematic errors to the simulated accelerometer measurements.

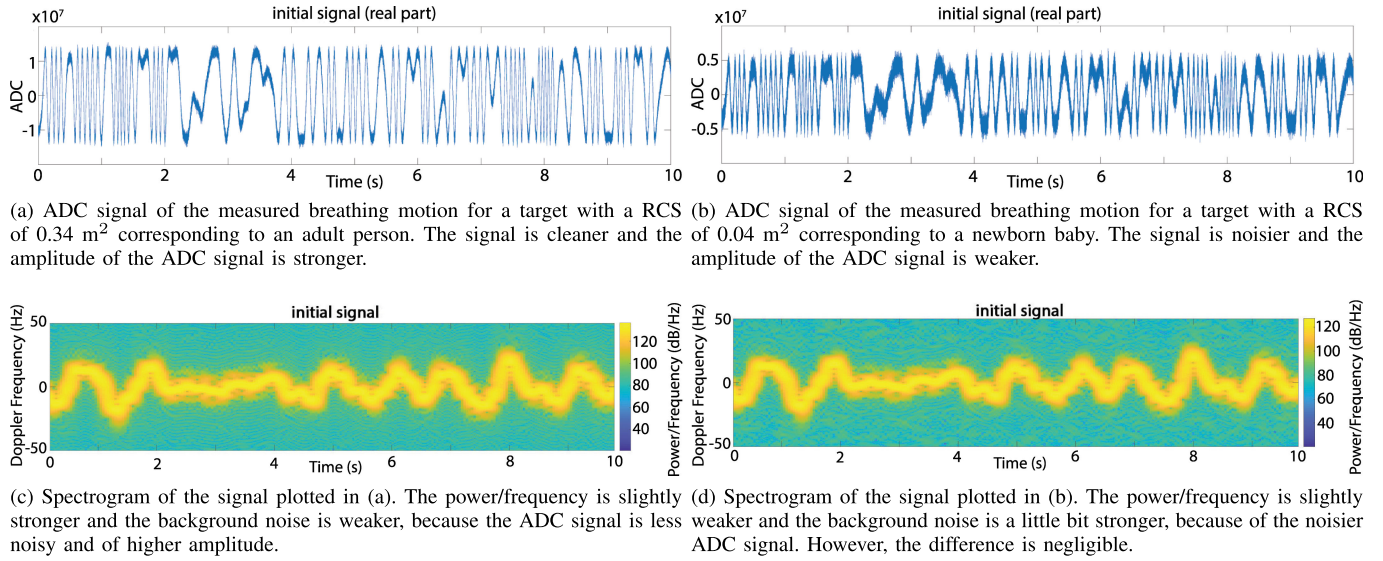


Fig. 3. Comparison between the simulated ADC signals and their resulting spectrograms for two identical breathing motions under the same road profile for two different RADAR cross section (RCS) values. The breathing frequency is $f = 0.95 \text{ Hz}$ and the breathing amplitude $\alpha = 0.0045 \text{ m}$. The RADAR measurement is simulated over a time period of 10 seconds. Both targets have, for both simulations, the same mass. Due to the high processing gain of the FFT, the noise in the raw signals are equally good distributed over all frequencies so that the resulting spectrograms are almost indistinguishable.

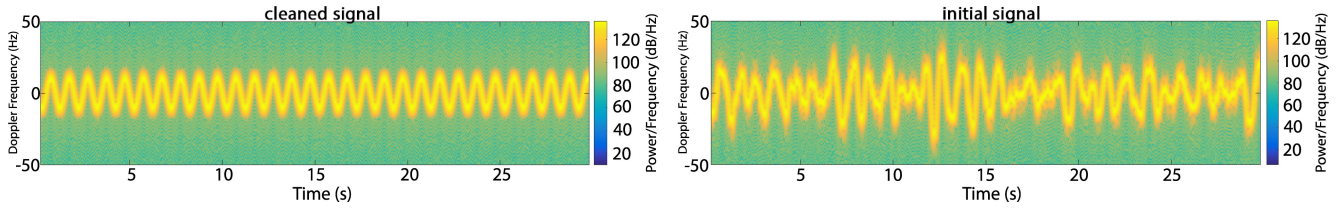


Fig. 4. Spectrogram of the received signal of the human chest with a RADAR cross section of 0.34 m^2 . Based on [15], the parameters chosen for the model are $m_C = 1200 \text{ kg}$, $S_C = 28000 \text{ Nm}^{-1}$, $D_C = 2500 \text{ kgs}^{-1}$, $m_W = 60 \text{ kg}$, $S_W = 134000 \text{ Nm}^{-1}$, $D_W = 700 \text{ kgs}^{-1}$, $m_U = 75 \text{ kg}$, $S_U = 4000 \text{ Nm}^{-1}$, and $D_U = 200 \text{ kgs}^{-1}$.

F. Simulation Example

We consider a road profile of class C, simulated with 1000 frequencies, using (2). We use a car velocity of 15 ms^{-1} , $m_C = 1200 \text{ kg}$, $S_C = 28000 \text{ Nm}^{-1}$, $D_C = 2500 \text{ kgs}^{-1}$, $m_W = 60 \text{ kg}$, $S_W = 134000 \text{ Nm}^{-1}$, $D_W = 700 \text{ kgs}^{-1}$, $m_U = 75 \text{ kg}$, $S_U = 4000 \text{ Nm}^{-1}$ and $D_U = 200 \text{ kgs}^{-1}$ as proposed in [15]. The seat displacement and the car-body displacement are simulated for a duration of 30 seconds by solving the system of differential equations (5) numerically. Additionally, we consider an interior RADAR observing a point target P undergoing motion along the z-direction and a respiratory motion along x-direction with breathing frequency 0.95 Hz and breathing amplitude 4.5 mm. Fig. 4a shows the spectrogram of the received signal from the point target P undergoing respiratory motion only. Fig. 4b shows the spectrogram of the received signal from the point target P undergoing superposition of the respiratory motion and the displacement along z-direction caused by the road profile. The respiratory motion is not visible due to the “noise” caused by the road profile. The corresponding accelerometer measurement is illustrated in Fig. 5.

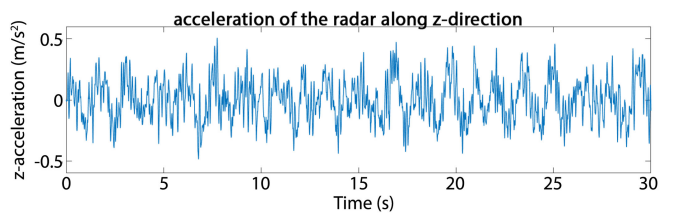


Fig. 5. Simulated accelerometer measurement for a road profile of roughness class C, obtained by storing the acceleration of the car-body during the simulation.

III. THE DENOISING METHOD

The observed point target P undergoes two motions simultaneously: the motion of interest (respiratory motion) and the second unwanted motion, caused by the displacement of the seat. Unfortunately, this unwanted motion disturbs the Doppler frequency considerably, so that we are no longer able to detect or monitor the breathing motion. In this section, we will present a method to denoise the signal shown in Fig. 4b, so that it reduces to the signal shown in Fig. 4a.

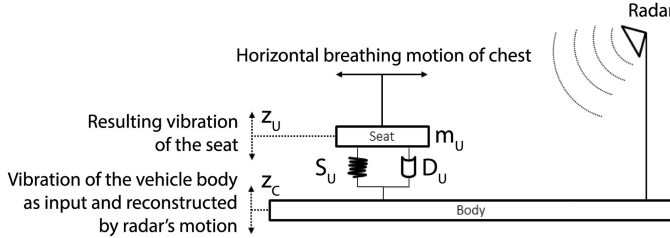


Fig. 6. One-spring model of a seat coupled to the car-body.

We propose to attach an accelerometer to the RADAR-based sensor, so that we can gain information about the vibrational motion and displacement of the car-body caused by exterior influences (car engine, street profile, wind gusts). This information is then used to reconstruct the displacement of the seat, which is then used to calculate its contribution to the Doppler frequency observed by the interior RADAR. Once this contribution is calculated, we can denoise the signal by removing this contribution. In this way we are left with a signal containing (almost) only the information about the respiratory motion.

A. Mechanical Reconstruction

We measured the motion of the RADAR-based sensor during the simulation by recording an accelerometer measurement. Consequently, by integrating the acceleration \ddot{z}_C , we can reconstruct the velocity \dot{z}_C and the position z_C of the car-body displacement up to a constant and a linear drift. This information can then be used to reconstruct the motion of the seat. For this, we no longer use the road profile as the driving force, but the vibrational motion of the car-body. Furthermore, in order to reconstruct the motion of the seat, we will use the one-spring model, as illustrated in Fig. 6, which is a reduced version of the three-spring model (5). The one spring model is governed by the differential equation:

$$m_U \ddot{z}_U + D_U \dot{z}_U + S_U z_U = D_U \dot{z}_C + S_U z_C. \quad (8)$$

In this case, the driving is given by the term $D_U \dot{z}_C + S_U z_C$, i.e. the motion of the car body, and the output of the differential equation is the displacement of the seat z_U .

In the reconstruction of the seat displacement, it is mandatory to know the (exact) mass of the passenger. For the moment, we assume that all system parameters are known.

Once the displacement of the seat is calculated, we can then compute the relative motion $z(t)$ between the seat $z_U(t)$ and the RADAR $z_C(t)$, since the RADAR sensor observes the relative motion of the target:

$$z(t) = z_C(t) - z_U(t). \quad (9)$$

In order to be in line with realistic conditions, we assume that no knowledge about initial conditions for the reconstruction (8) is available. However, this does not represent an issue for two reasons. First, a constant offset in the reconstruction of \dot{z}_C (resulting in the presence of an additional linear drift in z_C) does not affect the performance, since only instantaneous, relative changes have significant effect. Secondly, due to the fact that the underlying system constitutes a damped harmonic oscillator,

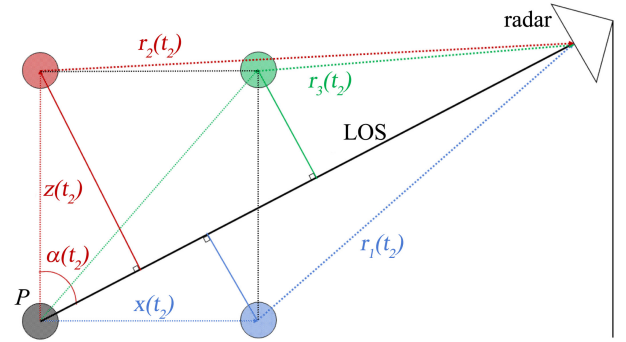


Fig. 7. Interior car RADAR observing a human chest (modeled by point target P) undergoing a respiratory motion $x(t)$ along the x -direction and vibrational motion $z(t)$ due to road roughness along the z -direction. $\alpha(t)$ is the instantaneous angle between $z(t)$ and the line of sight (LOS). Different components of the motion as well as their orthogonal projections onto the line of sight are illustrated: Respiratory motion only (blue), displacement due to road bumps along the z -direction (red), and both motions superimposed (green). $r_1(t)$, $r_2(t)$ and $r_3(t)$ are, respectively, the instantaneous distances between the human chest and the RADAR for the respiratory motion only, the z -displacement only and both motions superimposed.

the error in the reconstruction of \ddot{z}_U , \dot{z}_U , z_U caused by the lack of initial conditions will converge to zero over time.

B. The Denoising Method

We consider a point target P moving in the x - z plane from $(0,0)$ at $t = 0$ to $(x(t_2), z(t_2))$ at $t = t_2$, as illustrated in Fig. 7. The orthogonal projection of this motion onto the line of sight is then equal to the sum of the orthogonal projections of the motions along the x and z directions. We reconstruct the z -displacement of the seat, calculate the amount of relative motion $z(t)$ and then project it onto the line of sight. Let $\alpha(t)$ denote the instantaneous angle between $z(t)$ and the line of sight. The instantaneous projection is then given by

$$z(t) \cos(\alpha(t)). \quad (10)$$

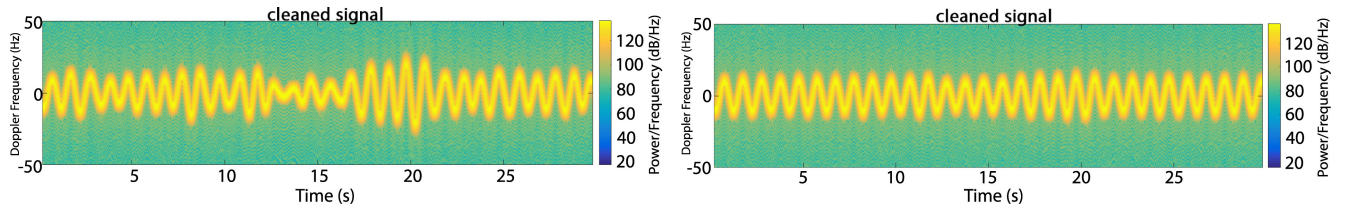
Consequently, we perform the denoising of the respiratory signal by multiplying the signal with

$$e^{-\frac{4\pi i}{\lambda} (r_3(t) - z(t) \cos(\alpha(t)))}, \quad (11)$$

where $e^{-\frac{4\pi i}{\lambda} r_3(t)}$ is the wave received by the interior RADAR observing the point target P undergoing both the respiratory and vibrational motion. $r_3(t)$ denotes the instantaneous distance between the RADAR and point P . At each time instance t , we have removed the vibrational contribution to the Doppler frequency by multiplying the received signal by a factor $e^{\frac{4\pi i}{\lambda} z(t) \cos(\alpha(t))}$, which cancels the vibrational effects and leaves only the breathing contribution.

The angle $\alpha(t)$ can be taken as a constant (which is not known a priori), since for every practical application the magnitude of the vibrational motion is much smaller than the typical distance of the target to the RADAR sensor. The (constant) value of α is chosen such that optimal signal denoising is achieved.

The robustness of the denoising method is proven in the next section, where we investigate the error introduced to the solution of the one-spring model by using an incorrect mass. Furthermore, the efficiency and the feasibility of the



(a) Using a 30% error for the passenger's mass and allowing for 5% production tolerances on the damping and stiffness constants for the reconstruction of the displacement of the seat along the z-direction using the one-spring model. (b) Using a 10% error for the passenger's mass and allowing for 5% production tolerances on the damping and stiffness constants for the reconstruction of the displacement of the seat along the z-direction using the one-spring model.

Fig. 8. Spectrogram of the denoised signal with uncertainties in the passenger's mass and in the damping and stiffness constants of the spring (e.g., due to production tolerances). We assumed a constant angle α for the projection onto the line of sight.

denoising method is demonstrated by the solution of an optimization problem.

C. Simulation Results

The acceleration of the RADAR-device was recorded during the simulation. We use this information to calculate the velocity and the position of the car-body displacement with respect to its position, without exterior influences. Once we have calculated these values, we use the one-spring model (8) to calculate the resulting seat displacement. We introduced a 5% error on the damping and stiffness constants, since in practice they might not be exactly known.

In order to perform successful denoising, all the system parameters need to be known - passenger's mass and the stiffness and damping parameters. If, for instance, one tries to perform the denoising method (11), with an incorrect value of passenger's mass, which differs from an actual mass by 30%, then the denoising method will not be completely successful, as depicted in Fig. 8a.

IV. MATHEMATICAL FOUNDATION OF THE MECHANICAL MODEL

A. General Mechanical Model

In this article, for the sake of simplicity, we applied a one-spring model, see Section II-B, and a three-spring model, see Section III-A, to simulate the vibrations of the seat and demonstrate the denoising method. More complex car models (that, for example, also include car rotations) can be employed without the loss of generality. In this section, we analyse the mathematical properties of such systems that are crucial for the denoising method and perform a sensitivity analysis of the proposed signal reconstruction.

A model describing a set of n coupled harmonic oscillators driven by an exterior force $\underline{F}(t)$ can be formulated by the vector differential equation [20],

$$\underline{\underline{M}}\ddot{\underline{z}} + \underline{\underline{D}}\dot{\underline{z}} + \underline{\underline{S}}\underline{z} = \underline{F}(t), \quad (12)$$

where a single underline denotes a vector, a double underline denotes a square matrix, and $\underline{z} = \underline{z}(t)$ and $\underline{F}(t)$ are \mathbb{R}^n -valued functions of time $t \in \mathbb{R}$. $\underline{z}(t)$ describes the displacement with respect to the equilibrium position. Here $\underline{\underline{M}}$ represents the mass matrix, $\underline{\underline{S}}$ the matrix of stiffness constants and $\underline{\underline{D}}$ the matrix

containing damping terms. All these matrices are real-valued square matrices of dimension n . In general, $\underline{\underline{M}}$, $\underline{\underline{D}}$, $\underline{\underline{S}}$ and $\underline{F}(t)$ are known, whereas the displacement \underline{z} , the velocity $\dot{\underline{z}}$ and the acceleration $\ddot{\underline{z}}$ are unknown. If $\underline{\underline{M}}$ is non-singular, then together with some standard initial conditions

$$\underline{z}(0) = \underline{z}_0 \quad \dot{\underline{z}}(0) = \dot{\underline{z}}_0, \quad (13)$$

the differential equation (12) has a unique solution [20]. Assuming that $\underline{\underline{M}}$ is regular, we can rewrite (12) in the form

$$\ddot{\underline{z}} = -\underline{\underline{M}}^{-1}\underline{\underline{S}}\underline{z} - \underline{\underline{M}}^{-1}\underline{\underline{D}}\dot{\underline{z}} + \underline{\underline{M}}^{-1}\underline{F}(t), \quad (14)$$

which can be transformed into a system of first order differential equations by setting $\underline{z}_1 = \underline{z}$ and $\underline{z}_2 = \dot{\underline{z}}$, $\underline{z}_1(0) = \underline{z}_0$, $\underline{z}_2(0) = \dot{\underline{z}}_0$ to yield

$$\frac{d}{dt} \begin{pmatrix} \underline{z}_1 \\ \underline{z}_2 \end{pmatrix} = \underline{\underline{K}} \begin{pmatrix} \underline{z}_1 \\ \underline{z}_2 \end{pmatrix} + \underline{\underline{G}}(t), \quad (15)$$

where

$$\underline{\underline{K}} = \begin{pmatrix} 0_{n,n} & \underline{\underline{I}}_n \\ -\underline{\underline{M}}^{-1}\underline{\underline{S}} & -\underline{\underline{M}}^{-1}\underline{\underline{D}} \end{pmatrix}, \quad \underline{\underline{G}}(t) = \begin{pmatrix} 0_{n,1} \\ \underline{\underline{M}}^{-1}\underline{F}(t) \end{pmatrix}, \quad (16)$$

where $\underline{\underline{I}}_n$ is the n -dimensional identity matrix and $0_{n,m}$ is the $n \times m$ dimensional zero matrix. This system of differential equations can be solved by using the matrix exponential function and Duhamel's formula. The solution is then given by [20]

$$\begin{pmatrix} \underline{z}_1 \\ \underline{z}_2 \end{pmatrix} = e^{t\underline{\underline{K}}} \begin{pmatrix} \underline{z}_0 \\ \dot{\underline{z}}_0 \end{pmatrix} + \int_0^t e^{(t-\tau)\underline{\underline{K}}} \underline{\underline{G}}(\tau) d\tau. \quad (17)$$

The solution of the homogeneous part of (15) is simply given by

$$\begin{pmatrix} \underline{z}_1 \\ \underline{z}_2 \end{pmatrix} = e^{t\underline{\underline{K}}} \begin{pmatrix} \underline{z}_0 \\ \dot{\underline{z}}_0 \end{pmatrix}. \quad (18)$$

The following proposition is an important tool to verify the stability of differential equation [20].

Proposition IV.1: For a general square matrix $\underline{\underline{A}}$, the following are equivalent

- 1) $\underline{\underline{A}}$ is asymptotically stable,
- 2) $\Re(\sigma(\underline{\underline{A}})) < 0$,
- 3) $e^{t\underline{\underline{A}}} \rightarrow 0$, $t \rightarrow \infty$,

where $\sigma(\underline{\underline{A}})$ is the spectrum of the matrix $\underline{\underline{A}}$ and \Re is the real part.

Consequently, since the homogeneous solution is proportional to $e^{t\bar{K}}$, where \bar{K} is a matrix whose eigenvalues have negative real part, after certain time period t , this will become negligible, and the final solution of the differential equation (15) will solely be given by the particular solution, as confirmed by simulations.

One can show that the eigenvalues of the matrix \bar{K} for the one-spring model are of the form

$$\frac{1}{2} \left(\pm \sqrt{\frac{D_U^2}{m_U} - 4 \frac{S_U}{m_U}} - \frac{D_U}{m_U} \right), \quad (19)$$

for which the radicand is always negative for the constants used in this article. Consequently, because of the term $-\frac{D_U}{m_U}$ for which the constants are always positive, the real part of the eigenvalues is always negative.

B. Sensitivity Analysis of the Spring Model

The reconstruction of the motion of the seat under the influence of a driving force depends on the knowledge of several parameters, in particular the passenger's mass. In this section, we want to analyse the robustness of the solution of the proposed reconstruction applied to higher dimensional systems of damped oscillators. First, this gives means to assess the reliability of the method for an actual application where certain tolerances have to be assumed. Secondly, it serves as basis for the solution of the optimization problem to determine the passenger's mass, described in Section V.

We analyse the deviation between the reconstructed and actual solutions arising from different parameters.

The compact form of (15) reads

$$\dot{z} - \underline{K}z = \underline{G}(t), \quad (20)$$

which can be reformulated using the vector-valued differential operator

$$P \left(\frac{\partial}{\partial t} \right) = \underline{\underline{I}_n} \frac{\partial}{\partial t} - \underline{\underline{K}}. \quad (21)$$

In the notions of pseudo-differential operators [21], this operator can be identified with the symbol

$$P(\xi) = -i\xi\underline{\underline{I}_n} - \underline{\underline{K}}. \quad (22)$$

Consider a function $\underline{G}(t)$ of the form

$$\underline{G}(t) = \int_{-a}^a \underline{H}(\xi) e^{-it\xi} d\xi, \quad (23)$$

described by some density function \underline{H} . The differential operator P acting on the function $\underline{G}(t)$ gives

$$P(\underline{G}, t) = \int_{-a}^a \left(-i\xi\underline{\underline{I}_n} - \underline{\underline{K}} \right) \underline{H}(\xi) e^{-it\xi} d\xi. \quad (24)$$

Thus, given that the right hand side of (20) has the form (23), we conclude that the solution is given by

$$\underline{z}(t) = \int_{-a}^a (-i\xi\underline{\underline{I}_n} - \underline{\underline{K}})^{-1} \underline{H}(\xi) e^{-it\xi} d\xi, \quad (25)$$

provided $-i\xi\underline{\underline{I}_n} - \underline{\underline{K}}$ is regular in the interval $[-a, a]$. This observation leads to an elegant error analysis for the reconstruction method proposed in the previous section. We assume that the road profile (2) is adequately approximated by a Fourier-type representation in a certain range:

$$z_R(t) = \int_{-a}^a H_R(\xi) e^{-it\xi} d\xi, \quad (26)$$

for some value of a and some density function H_R . Applying the above reasoning, we conclude that the excitations of all considered damped oscillators can be written as in (23). In particular, we deduce that one can write z_C on the right hand side of (8) as

$$z_C(t) = \int_{-a}^a H_C(\xi) e^{-it\xi} d\xi. \quad (27)$$

Using (15) and (16), the system of second order differential equations (8) can be recast as a system of differential equations of first order of the following form:

$$\begin{aligned} \begin{pmatrix} \dot{z}_1 \\ \dot{z}_2 \end{pmatrix} &= \begin{pmatrix} 0 & 1 \\ -M^{-1}S & -M^{-1}D \end{pmatrix} \begin{pmatrix} z_1 \\ z_2 \end{pmatrix} \\ &= \begin{pmatrix} 0 \\ 1 \end{pmatrix} \int_{-a}^a M^{-1} (D(-i\xi) + S) H_C(\xi) e^{i\xi t} d\xi, \end{aligned} \quad (28)$$

where the index U has been suppressed. According to the previously presented arguments, the corresponding solution is hence given by

$$\underline{z}_{sol}(t) = \int_{-a}^a \underline{H}(\xi) e^{-it\xi} d\xi, \quad (29)$$

where

$$\underline{H}(\xi) = [-i\xi I_2 - \underline{\underline{K}}]^{-1} M^{-1} [D(-i\xi) + S] H_C(\xi) \begin{pmatrix} 0 \\ 1 \end{pmatrix}.$$

Similar reasoning also holds for higher dimensional versions of the previous equation. We will now analyse the deviation between the exact solution \underline{z}_{sol} and a solution implied by deviations of the parameters $\underline{\underline{z}}_{sol}$. The deviation is given by

$$\underline{z}_{sol}(t) - \underline{\underline{z}}_{sol}(t), \quad (30)$$

where the first component is the error between the displacements and the second component is the error between the velocities. For instance, we consider deviations in the mass of the following form

$$\tilde{m}_U = m_U + \epsilon, \quad (31)$$

where m_U is the actual mass, and ϵ is the deviation. We derive the error between seat displacements $\underline{z}_{sol}(t) - \underline{\underline{z}}_{sol}(t)$ for the special case of the one-spring model:

$$\begin{aligned} \underline{z}_{sol}(t) - \underline{\underline{z}}_{sol}(t) &= \int_{-a}^a H_C(\xi) \begin{pmatrix} -\xi^2 \epsilon \\ i\xi^3 \epsilon \end{pmatrix} e^{-it\xi} \times \\ &\quad \frac{D_U(-i\xi) + S_U}{(S_U - \xi^2 m_U - i\xi D_U)(S_U - \xi^2(m_U + \epsilon) - i\xi D_U)} d\xi. \end{aligned} \quad (32)$$

From this, we can immediately prove that if $\epsilon \rightarrow 0$ (which corresponds to $\tilde{m}_U \rightarrow m_U$) that

$$\lim_{\epsilon \rightarrow 0} (\underline{z}_{sol}(t) - \tilde{\underline{z}}_{sol}(t)) = \begin{pmatrix} 0 \\ 0 \end{pmatrix}, \quad (33)$$

meaning that the z-displacement (and the z-component of the velocity) converges to the correct z-displacement when the estimated mass of the passenger converges to the actual mass of the passenger. This error estimation procedure not only proves the convergence, but it also enables us to obtain a reliable error estimation when using a somewhat different mass value of the passenger. Further, the error is bounded, controllable and it can be easily computed at each time instance.

V. PASSENGER WEIGHT ESTIMATION

In order to perform the RADAR signal denoising, it is mandatory to know the passenger's mass up to a certain accuracy. However, in practice, this is rarely available, especially, when the driver and/or passengers change. As we have shown in the previous example of Section III-C and as illustrated in Fig. 8, the denoising method works better the smaller the error in the passenger's mass estimation. In the following section, we will formulate and solve an optimization problem that aims to find a good approximation of the passenger's mass by using the previously explained denoising method. In Section IV-B the robustness of the solution of the one-spring model has been analysed, which justifies us to formulate an optimization problem.

A. The Cost Function

If we use an incorrect mass estimate for the passenger, the one-spring model will generate a seat displacement which is different from the actual one. Consequently, while denoising the signal, we will remove the incorrect Doppler contribution from the received signal, and in the worst case we will introduce even more noise in the signal. However, we have shown that the reconstructed seat displacement converges to the correct one when the mass deviation ϵ in (31) converges to zero. In order to describe the quality of the denoising method, we need to develop a mathematical model which quantifies how much the actual denoised signal differs from the perfectly denoised signal containing the signatures of breathing only. For the sake of simplicity, here we will assume that the breathing motions can be characterized by a perfect (constant amplitude and frequency) sinusoidal wave. However, our results can be generalized to different, more complex breathing patterns with a suitable choice for the cost function.

For the simplest case of sinusoidal breathing, the cost function will describe the degree of difference of the spectrogram of the denoised signal versus the spectrogram of a perfect sinusoidal wave. As a descriptive representation of the spectrogram, we will take, at each time instance, a representative frequency, which corresponds to the frequency with the maximal amplitude (since the spectrogram cannot provide a perfect time-frequency resolution). We will denote this by $spec_{max}$.

In order to define the cost function, we start by computing the local maxima max_{loc} and the local minima min_{loc} of $spec_{max}$.

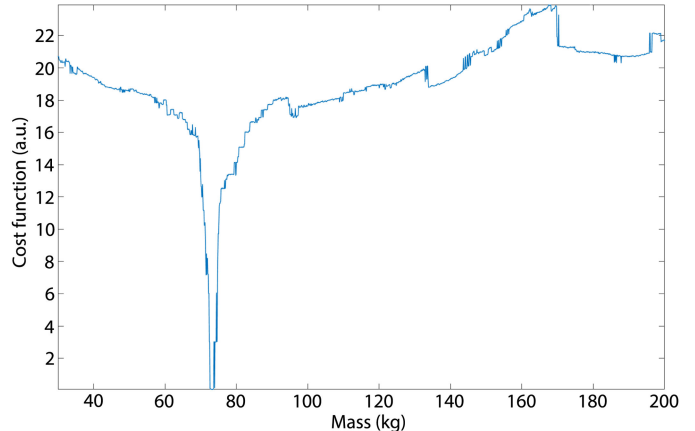


Fig. 9. Cost function evaluation for masses ranging from 30 kg up to 200 kg with a step size of 0.1 kg. The correct mass is 70 kg, but the optimal mass estimation is found around 73 kg, due to the introduction of tolerances of 5% on the damping and stiffness constants. The cost function is clearly not convex.

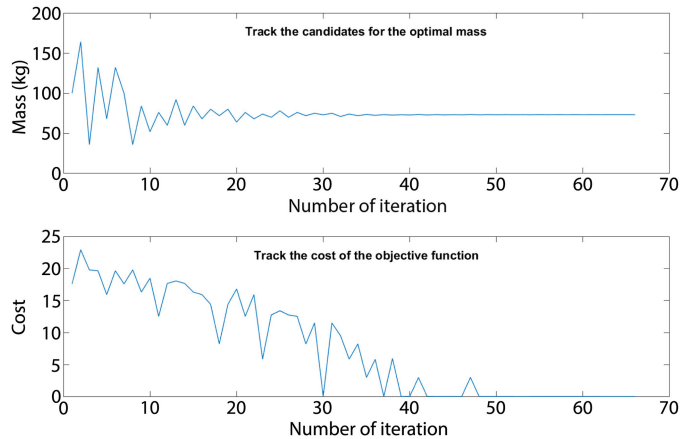


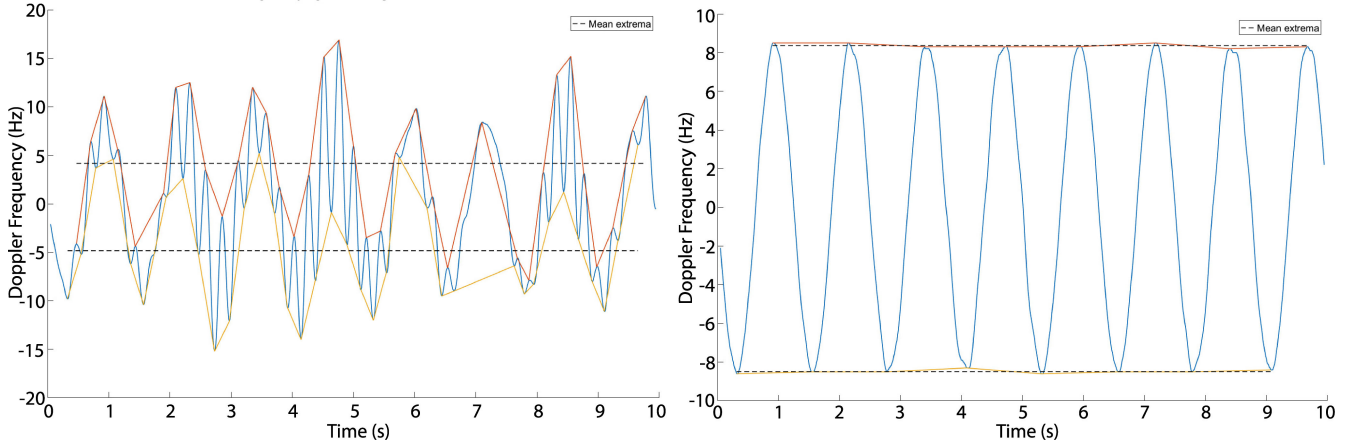
Fig. 10. Top: Evolution of the candidate choices for the passenger's mass. Bottom: The corresponding cost function evaluation. We used the MATLAB function *patternsearch* to minimize the cost function.

Next, we linearly interpolate the local maxima to get the upper envelope e_{max} and we linearly interpolate the local minima to get the lower envelope e_{min} .

For a perfect sinusoidal function, the local maxima and the local minima of $spec_{max}$ lie on two parallel horizontal lines. The following algorithm describes the steps in the implementation of one possible cost function to describe this characteristic mathematically:

- 1: Numerically differentiate the linear interpolations e_{max} and e_{min} of the local maxima and minima,
- 2: Sum up the absolute values of the numerical derivatives to get Σ ,
- 3: Minimize Σ .

If the local maxima/minima are on the same horizontal line, then the numerical derivative of each interpolation is zero at each time instance, due to the fact that we used a linear interpolation method.



(a) Using the starting value for the passenger mass of $m = 100$ kg. The evaluation of the cost function results in a cost of 17.6 a.u.. The Doppler frequency of the denoised RADAR signal is significantly different from the one of the actual breathing motion.
(b) Using the optimal mass of $m = 73.2$ kg. The evaluation of the cost function results in a cost of 0.076 a.u.. The Doppler frequency of the denoised RADAR signal does not significantly differ from the Doppler frequency of a breathing motion.

Fig. 11. In this example, the passenger mass used during the simulation is chosen to be $m = 70$ kg and we simulated the signal for 10 seconds. We have chosen the following realistic values for the mechanical constants: a damping constant of $D_U = 265 \text{ kg s}^{-1}$ and a stiffness constant of $S_U = 50000 \text{ N m}^{-1}$, both with 5% variance. Additionally, we introduced a possible error of 5% in the accelerometer measurement. The optimization algorithm will use the initial guess of $m = 100$ kg for the passenger's mass. Further, we assume that the mass value should be bound in the interval [30, 200] kg. Depicted is the spec_{\max} of the denoised signal using a damping constant of $D_U = 278.25 \text{ kg s}^{-1}$ and a stiffness constant of $S_U = 52500 \text{ N m}^{-1}$. The red curve represents the linear interpolation of the local maxima, whereas the yellow curve is the linear interpolation of the local minima. The two dotted lines represent the mean value of the local maxima and local minima, respectively.

It is important to remark that the cost function and the optimization problem are much more complicated than this rather simple error description. One needs to execute the steps in the following algorithm in order to solve the optimization problem and compute the cost function at each iteration:

- 1: **while** cost function not minimized **do**
- 2: Choose an estimate for the passenger mass m ,
- 3: Solve the differential equation (8) describing the one-spring model, using the mass estimate m , to get the z-displacement of the seat,
- 4: Clean the signal by using the z-displacement of the seat,
- 5: Compute the spectrogram, using short-time Fourier transform, of the denoised signal of point 4,
- 6: Use the result of point 5 and for each time instance take the frequency corresponding to the maximal amplitude to get spec_{\max} ,
- 7: Compute the local maxima and minima of spec_{\max} found in point 6,
- 8: Calculate the cost function,
- 9: **end while**
- 10: Use the mass m for which the cost function was minimized as the mass estimate of the passenger.

Since the minimization procedure is quite complex, it might be too expensive to find a gradient which can be used to minimize the cost function. Hence, in our simulations we used the derivative-free MATLAB functions *particleswarm*, *patternsearch* and *fminsearch* in order to minimize the cost function. Additionally, as it can be seen in Fig. 9, the cost function is not convex, which makes it numerically more challenging to

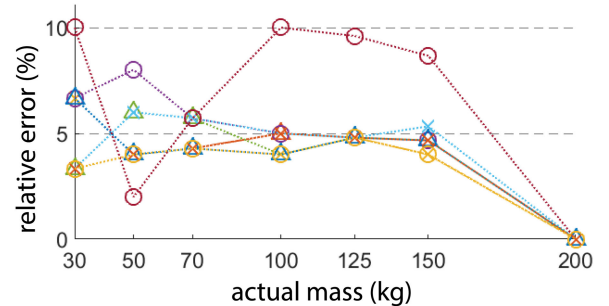
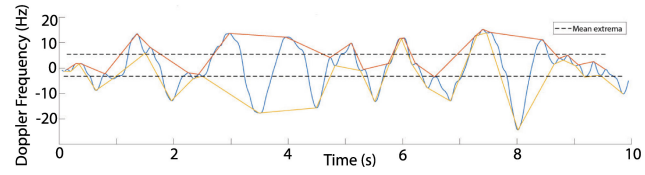


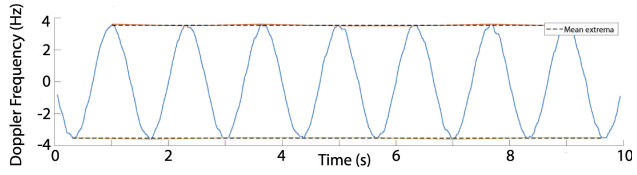
Fig. 12. Plot of the relative error in the estimated passenger's mass (using the optimization procedure described in Section V-A) as a function of actual passenger's mass. The different symbols, according to scenarios 1)-6),
○—Yellow ×—Yellow 1)
○—Red ×—Red 2)
○—Purple ×—Purple 1), 3), 5)
○—Blue ×—Blue 1), 4), 5)
×—Blue Δ—Blue 1), 3)
○—Blue Δ—Blue 1), 4), 6)
○—Red Δ—Red 1), 6)
○—Purple Δ—Purple 1), 5)
○—Blue Δ—Blue 1), 3), 6)
○—Green Δ—Green 1), 3), 6)
○—Blue Δ—Blue 1), 4), 6)
represent different combinations of errors introduced during the optimization procedure in order to make the scenario more realistic.

determine the global minimum. The rather complex resulting cost reflects the complexity of the underlying algorithm to find the minimum. Each step of the algorithm is sensitive to changes in the parameters and these sensitivities accumulate and influence each subsequent step. We have chosen one implementation to determine the passenger's mass, although other implementations might result in a smoother cost function.

Our cost function is to some extent tailored to our model of a sinusoidal breathing motion. Plenty of other cost functions, or variations of the one proposed in this work, are imaginable. For instance, the autocorrelation might be an additional ingredient to



(a) Using the starting value for the passenger mass of $m = 100$ kg. The evaluation of the cost function results in a cost of 78.6 a.u.. The Doppler results in a cost of 0.25 a.u.. The Doppler frequency of the denoised RADAR signal is significantly different from the signal does not significantly differ from the Doppler frequency of a breathing motion. Although the noise in the initial signal was not significant, when denoising the signal with a completely incorrect value for the passenger mass, the denoising will fail dramatically and introduce even more noise to the signal.



(b) Using the optimal mass of $m = 8.5$ kg. The evaluation of the cost function results in a cost of 0.25 a.u.. The Doppler frequency of the denoised RADAR signal does not significantly differ from the Doppler frequency of a breathing motion.

Fig. 13. In order to simulate the worst case scenario - that of a newborn baby, we chose the passenger mass to be $m = 8$ kg, the RCS of 0.04 m^2 , the breathing frequency $f = 0.75 \text{ Hz}$ and the breathing amplitude $\alpha = 2 \text{ mm}$ [18]. We simulated the signal for 10 seconds. The other parameters are chosen as in Fig. 11. The optimization algorithm will use the initial guess of $m = 100$ kg for the passenger's mass. Further, we assume that the mass value should be bound in the interval $[1, 200]$ kg. Depicted is the $spec_{max}$ of the denoised signal. The red curve represents the linear interpolation of the local maxima, whereas the yellow curve is the linear interpolation of the local minima. The two dotted lines represent the mean value of the local maxima and local minima, respectively.

quantify periodicity in the signal [22]. At the end, the expected breathing pattern gives a hint on how to tune the cost function in order to measure the efficiency of the denoising.

B. Example

In this section, we will demonstrate the previously explained optimization procedure on an example. For the simulation of the road profile we use a road roughness of ISO class C and a profile consisting of 1000 different frequency components. The breathing motion is simulated by

$$x(t) = 0.0045 \cos(2\pi \cdot 0.8 \cdot t), \quad (34)$$

where the breathing amplitude is chosen to be 4.5 mm and the breathing frequency is chosen to be 0.8 Hz. Our aim is to find an approximation of the passenger's mass using only the accelerometer measurement data and the denoising method of the RADAR signal as described in Section III-B.

If we reconstruct the displacement of the seat along the z-direction using the initial mass estimation of $m = 100$ kg, then the resulting $spec_{max}$ and the corresponding cost function evaluation can be found in Fig. 11a. In order to minimize the cost function, we used the MATLAB function *patternsearch*. The evolution of the different choices for the passenger's mass and the corresponding evaluations of the cost function can be found in Fig. 10. The optimum was found for 73.2 kg and the resulting Doppler frequency of the denoised RADAR signal is illustrated in Fig. 11b. The Doppler frequency of the denoised RADAR signal using the optimal mass estimation does not differ significantly from the Doppler frequency of the breathing motion (34). Furthermore, the relative error between the optimal mass and the correct passenger's mass is 4.58 %, which represents an accurate estimate for many applications (e.g., airbag deployment intensity).

C. Error Analysis

We formulated an optimization procedure to find an approximation for the passenger's mass. We performed this optimization procedure on many different simulated scenarios and

we investigated the relative error between the mass estimation found by the optimization procedure and the actual passenger's mass, which was input in the simulation. For a fixed road profile, we performed the simulations for different passenger masses in order to show that the success of the solution of the optimization problem does not depend on the passenger's mass. Namely, the passenger's mass was chosen in the set $m \in \{30, 50, 70, 100, 125, 150, 200\}$ kg. The interval of possible values for the passenger's mass for the minimizer was $[30, 200]$ kg. In order to model a realistic situation, we introduced different possible sources of error (e.g., due to production tolerances for car spring) and measurement resolutions:

- 1) 5% production tolerance in damping and stiffness constants,
- 2) 10% production tolerance in damping and stiffness constants,
- 3) 5% systematic error in accelerometer measurements,
- 4) 5% normally distributed error in accelerometer measurements,
- 5) 0.01 ms^{-2} resolution of accelerometer measurements,
- 6) 0.02 ms^{-2} resolution of accelerometer measurements.

Fig. 12 shows the relative error for the passenger's mass found using the optimization algorithm described in Section V-A, taking into account various production tolerances and finite measurement resolutions, scenarios 1)–6). We have found that the relative error for the mass estimate does not extend 10% for any of the (combined) cases 1)–6).

D. Worst Case Scenario: Denoising the Signal of a Newborn

So far we have only modelled adult passengers and consequently only considered a minimum possible weight of 30 kg. In this section, we want to briefly illustrate the worst case scenario of a newborn baby with a weight of less than 8 kg and a RCS of 0.04 m^2 , a breathing frequency of $f = 0.75 \text{ Hz}$ and a breathing amplitude of $\alpha = 2 \text{ mm}$ [18]. Fig. 14 illustrates the spectrogram of the noisy RADAR signal. Compared to the previous cases, the noise caused by the seat motion is less dominant, because the resulting passenger motion is smaller due to the lighter weight.

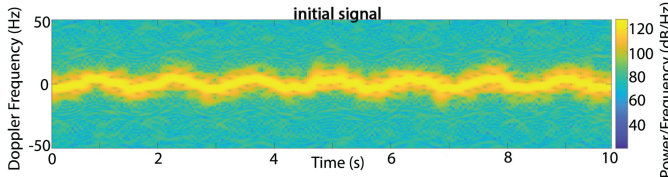


Fig. 14. Spectrogram of the received signal of the baby chest with a RADAR cross section of 0.04 m^2 , a breathing frequency of $f = 0.75 \text{ Hz}$ and a breathing amplitude of $\alpha = 0.002 \text{ m}$ as investigated in [18]. The baby's mass is chosen to be 8 kg. Based on [15], the parameters chosen for the model are $m_C = 1200 \text{ kg}$, $S_C = 28000 \text{ Nm}^{-1}$, $D_C = 2500 \text{ kgs}^{-1}$, $m_W = 60 \text{ kg}$, $S_W = 134000 \text{ Nm}^{-1}$, $D_W = 700 \text{ kgs}^{-1}$, $m_U = 75 \text{ kg}$, $S_U = 4000 \text{ Nm}^{-1}$, and $D_U = 200 \text{ kgs}^{-1}$. The noise is less dominant as in the previous examples, because of the light weight of the baby.

As in the previous section, we solve the introduced optimization problem to get an approximation for the mass of the baby. The optimum was found at 8.5 kg. The cost function evaluation for the optimal passenger mass estimation is represented in Fig. 13. Using the initial guess of 100 kg results in a very noisy signal, since the reconstructed seat motion is completely different from the seat motion bearing a baby weight. Hence, by removing the Doppler contribution of a much more dominant seat motion, we introduce a lot of noise to the signal.

VI. CONCLUSION

Monitoring vital signs in vehicle interior using a RADAR sensor becomes rather challenging when the vehicle is undergoing some vibrational motion caused, for example, by driving over street bumps. In this case, the observed target undergoes multiple motions, e.g., motion associated with vital sign observation (heart beat, breathing, pulse), and other, undesired motion caused by exterior influences which we would like to eliminate in order to perform vital sign passenger detection.

We introduced a mathematical framework and proposed to attach an accelerometer to the RADAR-based sensor, which enabled us to record its acceleration due to the motion caused by unwanted exterior effects. We used this information to reconstruct the motion of the seat and the passenger, which was then used to calculate the corresponding Doppler contribution. This Doppler contribution arising from the undesired vibrational motion due to external influences was then used to denoise the signal received by a RADAR-based sensor. After the denoising procedure the RADAR signal contained the signatures of the vital signs only (e.g., periodic breathing motion).

However, in order to denoise the signal efficiently, apart from knowing the constants describing the mechanical model of the car, we also need to know the mass of the passenger, which is, *a priori*, not known. Therefore, we have formulated and solved an optimization problem to find a good approximation of the passenger's mass. After denoising the received signal using the approximate value for the mass (found by the previously performed optimization procedure), one can then easily extract the passenger's vital sign signal.

A. Limitations

We would like to point out the simplifications and assumptions of our models. We assumed a constant vehicle velocity, and hence no vehicle acceleration, and a simplified “rigid human” model. We considered the vibrational motion only along a single direction; in practice we would need to consider all three degree of freedoms to account for all possible motions. Although we used a simplified mechanical car model (described by a set of 2nd order differential equations) to describe the car body and seat motion, we believe that a more complex model should not impact the feasibility of our method as long as the parameters of the mechanical model are known.

B. Discussion and Future Work

Further investigations and experimental verifications still need to be performed in order to validate the feasibility of the proposed techniques for practical applications. Although the three-spring model and the one-spring model are relatively simple models to describe the influence of the road profile on the vibrational motion inside the car, more complex models, e.g., [23] and [24], should not have an impact on the feasibility of the proposed methods, but rather make the computations lengthier. The directions for future work include considering more realistic breathing scenarios (variations in breathing amplitude and breathing frequency) and additional passenger movements (e.g., limb movement, bending).

In this work, the denoising technique relies on measurements received from a single accelerometer. As an extension of our work, one can also consider a system with (multiple) accelerometer(s) further attached to the seat(s), such that the seat acceleration, and hence displacement, can be measured directly. Additionally, the implementation of a Kalman filter [25], [26], [27] or moving horizon estimation [28] based algorithm could be investigated to reduce the uncertainty of many parameters in the vehicle interior, e.g., the damping and stiffness constants of the physical model. Furthermore, their implementation would lead to a better approximation of the mismatch between the accelerometer measurement with respect to the actual motion of the RADAR device. This could produce more reliable predictions for seat and passenger displacements that tend to be more accurate than those based on a single accelerometer measurement alone. In practice, this is performed by calculating a joint probability distribution over the variables for every time frame. As the general approach is not limited to continuous wave RADAR with fixed frequency and phase, future work could investigate the exploitation of advantageous properties of phase-modulated (PMCW) or frequency-modulated (FMCW) wave RADAR.

ACKNOWLEDGMENT

The authors would like to thank Xavier Antoine from the University of Lorraine, as well as Werner Bieck and Günther Gödert for useful discussions and support. We would also like to acknowledge IEE S.A. for resources during this project.

REFERENCES

- [1] A. Droitcour, V. Lubecke, J. Lin, and O. Boric-Lubecke, "A microwave radio for doppler radar sensing of vital signs," in *Proc. IEEE MTT-S Int. Microw. Symp. Dig.*, vol. 1, 2001, pp. 175–178.
- [2] A. Lazaro, D. Girbau, and R. Villarino, "Analysis of vital signs monitoring using an IR-UWB radar," *Progress Electromagn. Res.*, vol. 100, pp. 265–284, 2010.
- [3] J. Li, L. Liu, Z. Zeng, and F. Liu, "Advanced signal processing for vital sign extraction with applications in UWB radar detection of trapped victims in complex environments," *IEEE J. Sel. Topics Appl. Earth Observ. Remote Sens.*, vol. 7, no. 3, pp. 783–791, Mar. 2014.
- [4] V. M. Lubecke, O. Boric-Lubecke, A. Host-Madsen, and A. E. Fathy, "Through-the-wall radar life detection and monitoring," in *IEEE/MTT-S Int. Microw. Symp.*, 2007, pp. 769–772.
- [5] A. R. Diewald *et al.*, "Rf-based child occupation detection in the vehicle interior," in *Proc. 17th Int. Radar Symp.*, 2016, pp. 1–4.
- [6] G. Vinci, T. Lenhard, C. Will, and A. Koelpin, "Microwave interferometer radar-based vital sign detection for driver monitoring syst," in *Proc. IEEE MTT-S Int. Conf. Microw. Intell. Mobility*, 2015, pp. 1–4.
- [7] G. Carenza and J. Landwehr, "Radar sensing of vehicle occupancy," U.S. Patent 20170282828, Mar. 17, 2016. [Online]. Available: <https://encrypted.google.com/patents/WO2016038148A1?cl=da>
- [8] C. Gu and C. Li, "Assessment of human respiration patterns via noncontact sensing using doppler multi-radar system," *Sensors*, vol. 15, no. 3, pp. 6383–6398, 2015.
- [9] M. E. Farmer and A. K. Jain, "Occupant classification system for automotive airbag suppression," in *Proc. IEEE Comput. Soc. Conf. Comput. Vision Pattern Recognit.*, vol. 1, 2003.
- [10] V. C. Chen, F. Li, S.-S. Ho, and H. Wechsler, "Micro-doppler effect in radar: Phenomenon, model and simulation study," *IEEE Trans. Aerosp. Electron. Syst.*, vol. 42, no. 1, pp. 2–21, Mar. 2006.
- [11] D. L. Donoho, "De-noising by soft-thresholding," *IEEE Trans. Inf. Theory*, vol. 41, no. 3, pp. 613–627, 1995.
- [12] MATLAB, Phased Array System Toolbox. (2019). [Online]. Available: <https://nl.mathworks.com/products/phased-array.html>
- [13] W. Kester, *Mixed Signal and DSP Design Techniques*. Elsevier, 2002.
- [14] F. Tyan, Y.-F. Hong, S.-H. Tu, and W. S. Jeng, "Generation of random road profiles," *J. Adv. Eng.*, vol. 4, no. 2, pp. 151–156, Apr. 2009.
- [15] C. Patel, P. Gohil, and B. Borhade, "Modelling and vibration analysis of a road profile measuring system," *Int. J. Automot.. Mech. Eng.*, vol. 1, no. 1, pp. 13–28, 2010.
- [16] W. Abbas, A. Emam, S. Badran, M. Shebl, and O. Abouelatta, "Optimal seat and suspension design for a half-car with driver model using genetic algorithm," *Intell. Control Autom.*, vol. 4, pp. 199–205, 2013.
- [17] M. Cavagnaro, E. Pittella, and S. Pisa, "Numerical evaluation of the radar cross section of human breathing models," *Appl. Comput. Electromagn. Soc. J.*, vol. 30, pp. 1354–1359, 12 2015.
- [18] D. Tatarinov, U. Karahasanovic, U. Schröder, and O. Gomez, "Time dependent detection analysis for a virtual radar analysis tool," in *Proc. 18th Int. Radar Symp.*, 2017, pp. 1–9.
- [19] J. Fortuny-Guasch and J.-M. Chareau, "Radar cross section measurements of pedestrian dummies and humans in the 24/77 GHz frequency bands: Establishment of a reference library of RCS signatures of pedestrian dummies in the automotive radar bands," European Commission, Ispra, Italy, Tech. Rep. EUR 25762 EN, 2013.
- [20] K. Veselić, *Damped Oscillations of Linear Systems: A Mathematical Introduction* (Lecture Notes in Mathematics). Berlin, Germany: Springer, 2011.
- [21] M. E. Taylor, "Pseudodifferential operators," in *Partial Differential Equations II*. Springer, 1996, pp. 1–73.
- [22] B. Lohman, O. Boric-Lubecke, V. Lubecke, P. Ong, and M. Sondhi, "A digital signal processor for doppler radar sensing of vital signs," *IEEE Eng. Medicine Biol. Mag.*, vol. 21, no. 5, pp. 161–164, Sep./Oct. 2002.
- [23] S. Kim, S. White, A. Bajaj, and P. Davies, "Simplified models of the vibration of mannequins in car seats," *J. Sound Vib.*, vol. 264, no. 1, pp. 49–90, 2003.
- [24] M. Unterreiner, "Modellbildung und simulation von fahrzeugmodellen unterschiedlicher komplexität," Ph.D. dissertation, Maschinenbau und Verfahrenstechnik, Fakultät für Ingenieurwissenschaften, Universität Duisburg-Essen, 2013.
- [25] R. G. Brown *et al.*, *Introduction to Random Signals and Applied Kalman Filtering*, vol. 3. New York, NY, USA: Wiley, 1992.
- [26] V. T. Dang, "An adaptive kalman filter for radar tracking application," in *Proc. Microw., Radar Remote Sens. Symp.*, 2008, pp. 261–264.
- [27] Y. Chan, A. Hu, and J. Plant, "A Kalman filter based tracking scheme with input estimation," *IEEE Trans. Aerosp. Electron. Syst.*, vol. AES-15, no. 2, pp. 237–244, Mar. 1979.
- [28] J. B. Rawlings, "Moving horizon estimation," in *Encyclopedia of Systems and Control*. London, U.K.: Springer-Verlag, 2013, pp. 1–7.

Authors' photograph and biography not available at the time of publication.